Steady three-dimensional Streaks and their Optimal Growth in a Laminar Separation Bubble

O. Marxen[1], U. Rist[1], and D. Henningson[2]

[1] Universität Stuttgart, Institut für Aerodynamik und Gasdynamik (IAG)
Pfaffenwaldring 21, D-70550 Stuttgart, Germany,
[2] Department of Mechanics, Royal Institute of Technology (KTH)
SE-100 44 Stockholm, Sweden
olaf.marxen@iag.uni-stuttgart.de

Summary

A laminar separation bubble is formed in a region of adverse pressure gradient on a flat plate by a separating boundary layer that undergoes transition, finally leading to a reattached turbulent boundary layer. Linear amplification of steady three-dimensional disturbances in the flow before separation and in the laminar part of such a separation bubble is studied by means of direct numerical simulation and an adjoint-based optimization technique suited to study spatial optimal transient growth. The steady disturbances develop as streaks following their excitation in the region of favorable pressure gradient. At separation and inside the bubble, numerical and experimental results show good agreement with theoretical predictions for the optimal disturbance. The growth rate of the steady disturbance is seen to possess a maximum around the spanwise wave length that was found to be a preferred one in the corresponding experiment.

1 Introduction

Transition to turbulence in a two-dimensional separated boundary layer often leads to reattachment of the turbulent boundary layer and the formation of a laminar separation bubble (LSB). In many cases, the transition process is solely governed by a strong amplification of *fluctuating* disturbances. However, for environments with higher free-stream disturbance levels or if a strong favorable pressure gradient precedes the adverse pressure gradient, *steady* 3-d disturbances are sometimes observed inside the LSB. Research of bypass transition in zero pressure-gradient boundary layers revealed the possibility of transient growth of such disturbances that are often referred to as streaks [1, 2]. Despite the notation "bypass transition", amplification of these perturbations can still be a linear process [3].

While it is now commonly accepted that the process of formation of 3-d streaks in flat-plate boundary layers can be caused by transient growth, the appearance of 3-d perturbations in separated flows was in the past frequently attributed to a Görtler instability[4, 5]. Amplification of corresponding streamwise vortices is a result of

streamline curvature around the separation location. Presence of streaks in conjunction with separated flows was experimentally observed in [6], but not related to transient growth. Their development in LSBs and their relation to transient growth has only recently been studied experimentally and theoretically [7].

This work is a continuation and extension of a DNS study on 3-d steady disturbances that was published in [8]. Therefore, a brief summary of the findings of [8] shall be given here. Four different ways of exciting a steady perturbation either directly via blowing/suction at the wall or by non-linear generation were applied in that study. Even though all cases showed the same finally disturbance shape and growth rate inside the LSB, overall best agreement with a corresponding experiment could be achieved by forcing a pair of oblique waves in the region of favorable pressure gradient. In that case, an initial streamwise vortex relaxed into a streak downstream after a long region of transient behavior.

2 Description of the Flow Field

The reference case is chosen according to a set-up that has been studied extensively by means of numerical and experimental methods[9, 10]. A flat plate is mounted in the free stream of the test section of a laminar water tunnel. A streamwise pressure gradient is imposed locally on the flat-plate boundary layer by a displacement body, inducing a region of favorable pressure gradient followed by a pressure rise (Fig. 1). In the region of adverse pressure gradient (APG, $\breve{x} > 0m$), a laminar separation bubble develops. A rough estimate of the pressure gradient parameter (see [11]) for the APG-region gives P=$\breve{\delta}_2/\breve{\nu} \cdot \partial\breve{u}_{slip}/\partial\breve{x}|_{Separation} \approx -0.23$. The transition experiment is performed with controlled disturbance input. Perturbations are forced at x=-0.23 by an oscillating wire with regularly placed 3-d roughness elements (spacers) underneath the wire.

Non-dimensionalization is achieved by a reference velocity $\breve{U}_{ref}$=0.15 m/s $\approx 1.2 \cdot \breve{U}_\infty$ and a reference length $\breve{L}_{ref}$=$^2/_3\, m$ ($\approx$ length of the body $\breve{L}_{DB}^{Exp}$=$0.69m$), resulting in a Reynolds number Re_{global}=10^5 in water. At the streamwise position of the inflow boundary x_{ifl}=-0.6, the observed boundary-layer profile can be approximated by a Falkner-Skan similarity solution with Re_{δ_1}=900 and β_H=1.03.

To obtain a base flow for subsequent stability calculations (of theoretical nature or based on the Navier-Stokes equations in disturbance formulation), a DNS with controlled disturbance input had to be carried out to generate a laminar separation bubble close in shape to the experimental one. General physical parameters of the flow were chosen to match the set-up described above as accurately as possible. Details of this precursor computation can be found in [12].

The resulting unsteady flow field was averaged in time and subsequently used as a base flow with a height y_{max}=0.12. Fig. 2 shows the streamwise evolution of some boundary-layer parameters to provide an impression on the flow field. As argued in [8, 12], for the laminar part of the LSB the flow field can be well assumed to be a sufficiently accurate solution to the steady Navier-Stokes equations.

3 Theoretical and Numerical Methods

3.1 Theoretical Method to Compute Optimal Disturbances

The present paper puts its focus on physical aspects regarding the disturbance development. Therefore, the applied methods are described only very briefly. For theoretical investigations, an iterative adjoint-based optimization algorithm is applied. The method is based on the linearized boundary-layer equations. It serves to maximize the kinetic disturbance energy at the downstream position x_1 for a given initial energy at the inflow x_0. Details of the applied method can be found in [13, 14].

In wall-normal direction a spectral method based on Chebychev polynomials with 106 collocation points was used, while the second-order marching procedure in streamwise direction involved 173 steps for the longest domain (reaching from x_0=-0.6 to x_1=0.33). Five different streamwise stations were used as inflow position (x_0=-0.6, -0.45,-0.3,-0.15,0, respectively), while the outflow was kept fixed at x_1=0.33.

If the downstream location for the optimization procedure, i.e. for the theoretical method, is extended beyond $x \approx 0.33$, convergence can not be achieved anymore. This seems to be related to the reverse-flow of the base flow profile, since artificially setting this reverse flow to zero allows to compute through the entire separation bubble *without* giving a visible change in the results up to x=0.33.

3.2 Numerical Method for Direct Numerical Simulations

Spatial direct numerical simulation of the three-dimensional unsteady incompressible Navier-Stokes equations in disturbance formulation serves to compute the disturbance development in the flow field described above. The method uses finite differences of fourth/sixth-order accuracy on a Cartesian grid for downstream (N=1794) and wall-normal (M=241) discretization [15]. Grid stretching in wall-normal direction allows to cluster grid points near the wall. In spanwise direction, a spectral ansatz is applied (K=5). To reduce computational effort, spanwise symmetry is assumed for calculations. An explicit fourth-order Runge-Kutta scheme is used for time integration. The domain for direct simulations covers the streamwise interval $x \in [-0.6, 0.6182]$. Upstream of the outflow boundary a buffer domain starting at $x \approx 0.45$ smoothly returns the flow to a steady laminar state.

Disturbances are forced via blowing and suction at the wall through a disturbance strip $x \in [-0.4268, -0.3398]$. Similarly to case B_{11} of [8], a pair of unsteady oblique 3-d perturbations $A_v(1, \pm 1)$=$1.164 \cdot 10^{-2}$ is forced in the disturbance strip. The fundamental frequency was β_0=30.7 and the fundamental spanwise wavenumber γ_0=72.0. As demonstrated in [8], such forcing results in an immediately decoupled steady mode $(0, 2)$ that is then linearly amplified. As for a linearized Navier-Stokes calculation, no steady-state solution can be obtained anymore for an integration domain where the useful region extends further than $x \approx 0.45$.

4 Results

A double Fourier transform in time and spanwise direction of data sets from measurements or computations yields disturbance amplitudes and phases. Below, the notation (h, k) will be used to specify the modes, with h and k denoting wavenumber coefficients in time and spanwise direction, respectively.

The issue of optimal growth was not explicitly addressed in [8], but results presented there already allow a short discussion of this matter. If we focus on the disturbance evolution in the four small-amplitude cases B_{xx} of [8] and consider only the (decoupled) linear evolution of the steady disturbance slightly downstream of the disturbance strip, we observe (Fig. 3, left) that the perturbation for case B_{11} possess the lowest initial amplitude for the streamwise velocity $\hat{u}'$ – note that the forcing amplitudes were adjusted so that they reach the same final state. Even if we would consider as a criterion the (kinetic) energy instead of the $\hat{u}'$-amplitude, still case B_{11} would give the optimal growing perturbation, since in all cases $\hat{v}', \hat{w}' \ll \hat{u}'$. For that reason, below we will deal only with the case of an excitation by an oblique pair of waves as described above. In sec. 4.1, a comparison with theoretical results is discussed while sec. 4.2 investigates the influence of the spanwise wave length.

4.1 Optimal Growth: DNS and Theory

Results of the theoretical optimization procedure for all the considered inflow positions x_0 are compared with numerical results in Fig. 3 (left). Good agreement of theoretical and DNS results is observed for the streamwise disturbance velocity component, if the inflow position for theoretical calculations is chosen upstream of the disturbance strip in the DNS. Inside the separation bubble, DNS as well as theoretical results become independent on the initial (in x) condition. However, for $x > 0.225$, i.e. inside the LSB, the theoretical prediction gives slightly larger growth rates compared to the DNS. Wall-normal and spanwise velocity components from theory also agree well with DNS (Fig. 3, right), even though the largest differences can be seen in the wall-normal component $\hat{v}'$.

The reason for the mentioned differences are due to different shapes of the wall-normal amplitude functions. These are given in Fig. 5 for three different streamwise locations (from left to right) and all three velocity components (from top to bottom). Similar to transient growth in a Blasius boundary-layer, an initial streamwise vortex (Fig. 5, x=-0.15) relaxes into a streak inside the LSB (x=0.3). Even though theoretical and DNS results possess a slightly different amplitude function initially, inside the separation bubble an almost perfect matching is observable.

As pointed out before (sec. 3.1), downstream of $x \approx 0.33$ theoretical computations fail to converge, but DNS results still show good agreement with the experimental data (Fig. 3, right and Fig. 5 for x=0.405). This hints at the possibility of elliptic effects, not captured by the boundary-layer equations, to set in. However, additional research is necessary for further clarification.

4.2 Influence of the Spanwise Wave Length

A free parameter neglected in the study [8] shall be investigated here: the spanwise wave number. Motivation of such a study comes from the question why in the experiment – of all spanwise wave lengths – the one corresponding to mode $(0, 2)$ in the present nomenclature appears to be a preferred wave length of the set-up. In the experiment, the wave length was chosen by 'trial-and-error', i.e. the length of, and gap between, the spacers (see Fig. 1) was varied until the most regular vortical structures appeared [16, 9, 10]. These showed only a weak deviation from a sinusoidal shape in spanwise direction around the separation location.

Fig. 4 shows results for the entire investigated parameter space. Focus is put on the x-positions that are located in the region of adverse pressure gradient (x=0.15) and at separation (x=0.225). As for the theoretical results, a local maximum in amplification rate (Fig. 4, left) occurs for a wave number close to mode $(0, 2)$, while the DNS results possess such a maximum only for x=0.3 (not shown). Results for very small spanwise wave numbers ($\gamma < 72$) become inaccurate due to too low integration domains in wall-normal direction.

Despite the amplification rates from DNS being largest for small spanwise wave numbers (Fig. 4, left) in the present scenario, it becomes clear that in particular these perturbations experience a strong penalty in absolute amplitude (Fig. 4, right). The reason for this lies in the consideration of transient growth along x (and in case of DNS also receptivity matters) that is taken into account only in the latter case.

5 Conclusion

The present study sheds some light on the origin and linear evolution of steady, spanwise-harmonic perturbations in a laminar separation bubble. All calculations discussed are based on a case for which a profound experimental data base exists.

Good agreement of DNS, theory, and measurements suggests that inside the separation bubble, indeed the optimal steady three-dimensional disturbance could be observed in the present case. Furthermore, the experimentally determined spanwise wave number was confirmed to be the most preferred one of the whole set-up.

Acknowledgments: Financial support of this research by the Deutsche Forschungsgemeinschaft DFG under grant Wa 424/19–1 and Ri 680/10–1 and by the Deutsche Akademische Austauschdienst („Projektbezogener Personenaustausch Schweden") is gratefully acknowledged. Olaf Marxen appreciates the hospitality at the Department of Mechanics (KTH Stockholm) during his visit there and thanks Ori Levin for giving him an introduction to his code used in this paper for the theoretical optimization. We thank Matthias Lang for providing detailed experimental results.

References

[1] Henningson, D.S.: Bypass transition and linear growth mechanisms. In Benzi, R., ed.: Advances in Turbulence V, Kluwer Academic Publishers, Dordrecht, Boston, London (1995) 190–204

[2] Reshotko, E.: Transient growth: A factor in bypass transition. Phys. Fluids **13** (2001) 1067–1075
[3] Henningson, D.S., Reddy, S.C.: On the role of linear mechanisms in transition to turbulence. Phys. Fluids **6** (1994) 1396–1398
[4] Inger, G.: Three-dimensional heat- and mass transfer effects across high-speed reattaching flows. AIAA Journal **15** (1977) 383–389
[5] Wilson, P.G., Pauley, L.L.: Two- and three-dimensional large-eddy simulations of a transitional separation bubble. Phys. Fluids **10** (1998) 2932–2940
[6] Watmuff, J.H.: Evolution of a wave packet into vortex loops in a laminar separation bubble. J. Fluid Mech. **397** (1999) 119–169
[7] Boiko, A.V.: Development of a stationary streak in a local separation bubble. Technical Report IB 224–2002 A04, German Aerospace Center (DLR), Institute for Fluid Mechanics, Göttingen (2002)
[8] Marxen, O., Rist, U., Wagner, S.: Effect of Spanwise-Modulated Disturbances on Transition in a Separated Boundary Layer. AIAA Journal **42** (2004) 937–944
[9] Lang, M., Rist, U., Wagner, S.: Investigations on controlled transition development in a laminar separation bubble by means of LDA and PIV. Experiments in Fluids **36** (2003) 43–52
[10] Lang, M.: Experimentelle Untersuchungen zur Transition in einer laminaren Ablöseblase mit Hilfe der Laser-Doppler-Anemometrie und der Particle Image Velocimetry. Dissertation, Universität Stuttgart (2005)
[11] Gaster, M.: The structure and behaviour of laminar separation bubbles. AGARD CP–4 (1966) 813–854
[12] Marxen, O.: Numerical Studies of Physical Effects Related to the Controlled Transition Process in Laminar Separation Bubbles. Dissertation, Universität Stuttgart (2005)
[13] Andersson, P., Berggren, M., Henningson, D.S.: Optimal disturbances and bypass transition in boundary layers. Phys. Fluids **11** (1999) 134–150
[14] Levin, O., Henningson, D.S.: Exponential vs algebraic growth and transition prediction in boundary layer flow. Flow, Turbulence and Combustion **70** (2003) 183–210
[15] Kloker, M.: A robust high-resolution split-type compact FD scheme for spatial direct numerical simulation of boundary-layer transition. Appl. Sci. Res. **59** (1998) 353–377
[16] Lang, M., Marxen, O., Rist, U., Wagner, S.: Experimental and Numerical Investigations on Transition in a Laminar Separation Bubble. In Wagner, S., Rist, U., Heinemann, H.J., Hilbig, R., eds.: New Results in Numerical and Experimental Fluid Mechanics III. Volume 77 of NNFM., Springer, Heidelberg (2001) 207–214

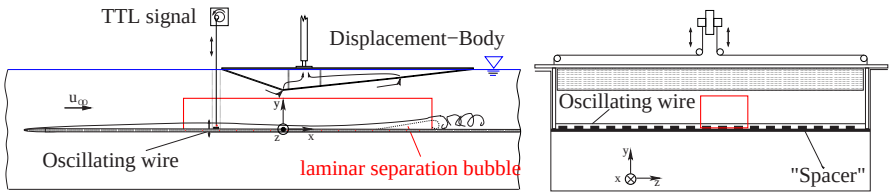

Figure 1 Configuration for the experiment by Lang et al. [9, 10]. The integration domain used for DNS and theory is indicated by a box (not to scale).

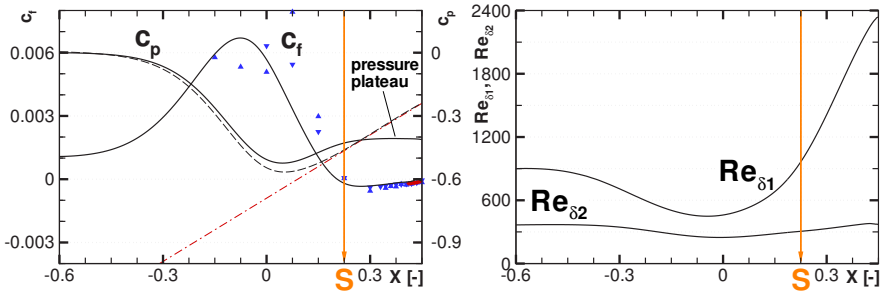

Figure 2 Coefficients for surface pressure c_p, skin friction c_f (left), and Reynolds numbers Re_{δ_1} and Re_{δ_2} (right). Comparison of DNS (solid lines), slip-flow results $c_{p,slip}$ (dashed line), and measurements (symbols).

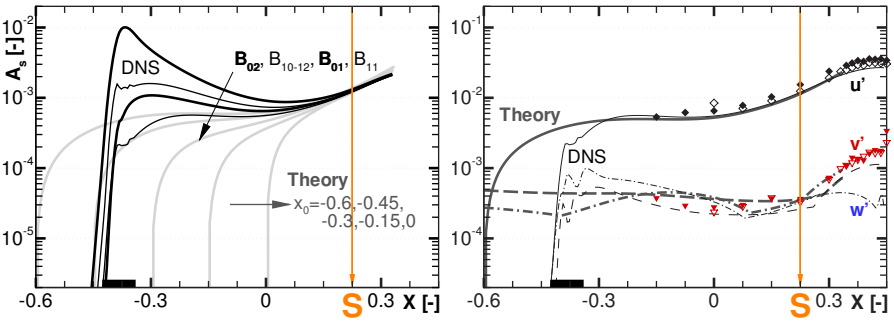

Figure 3 Amplification curves for the maximum (in y) streamwise (solid), wall-normal (dashed), and spanwise (dash-dotted) velocity fluctuation $|\hat{s}'^{(0,2)}_{max}|$. Left: all cases B_{xx} of [8] (dark lines) together with theoretical results for x_0=$-0.6, -0.45, -0.3, -0.15, 0$ (light lines). Right: DNS (thin lines) and theoretical results for x_0=-0.6 (thick lines) together with two different measurements (symbols).

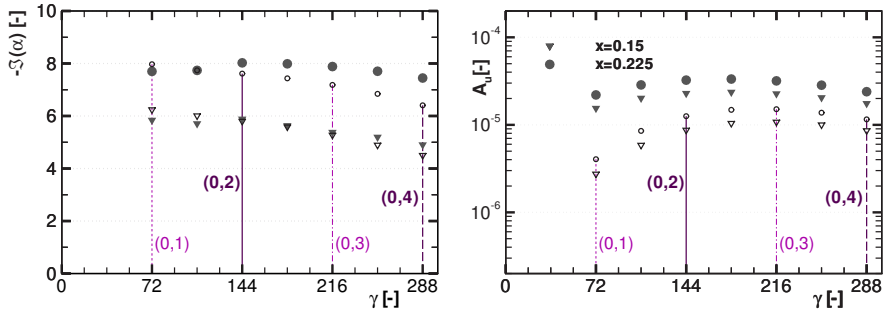

Figure 4 Left: Amplification rate $\Im(\alpha)$ vs. spanwise wave number γ for x=0.15 (triangles), 0.225 (circles) from DNS (open symbols) and theory (x_0=-0.6, filled symbols). Right: Maximum (in y) absolute amplitude $|\hat{u}'_{max}|$ vs. wave number γ at x=0.15 (triangles), 0.225 (circles) for equal forcing in DNS (strip interval $x \in [-0.4268, -0.3398]$, $A_v^{(1,k)}$=$5 \cdot 10^{-3}$) or for equal initial kinetic energy $\int(\hat{v}'^2 + \hat{w}'^2)dy$=$0.625 \cdot 10^{-8}$ in the theory.

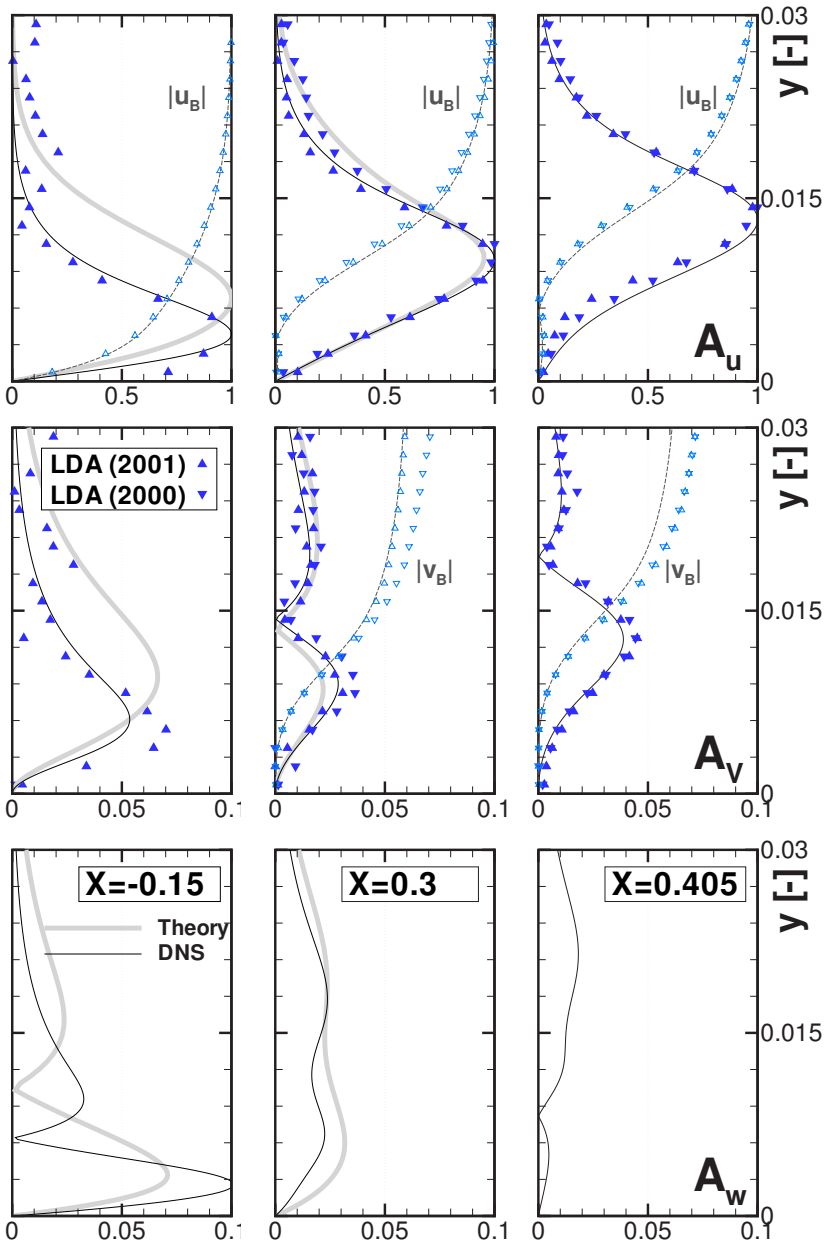

Figure 5 Velocity amplitudes $|\hat{u}'|$, $|\hat{v}'|$, $|\hat{w}'|$ (from top to bottom) of **mode** $(0, 2)$**,** normalized by their respective $|\hat{u}'_{max}|$. Comparison of results from DNS (thin line) and theory (x_0=-0.6, thick line) with two different measurements (symbols, as far as available) for x=-0.15, 0.3, 0.405 (from left to right). Base-flow quantities u_B, v_B are also shown.